CHALMERS
UNIVERSITY OF TECHNOLOGY

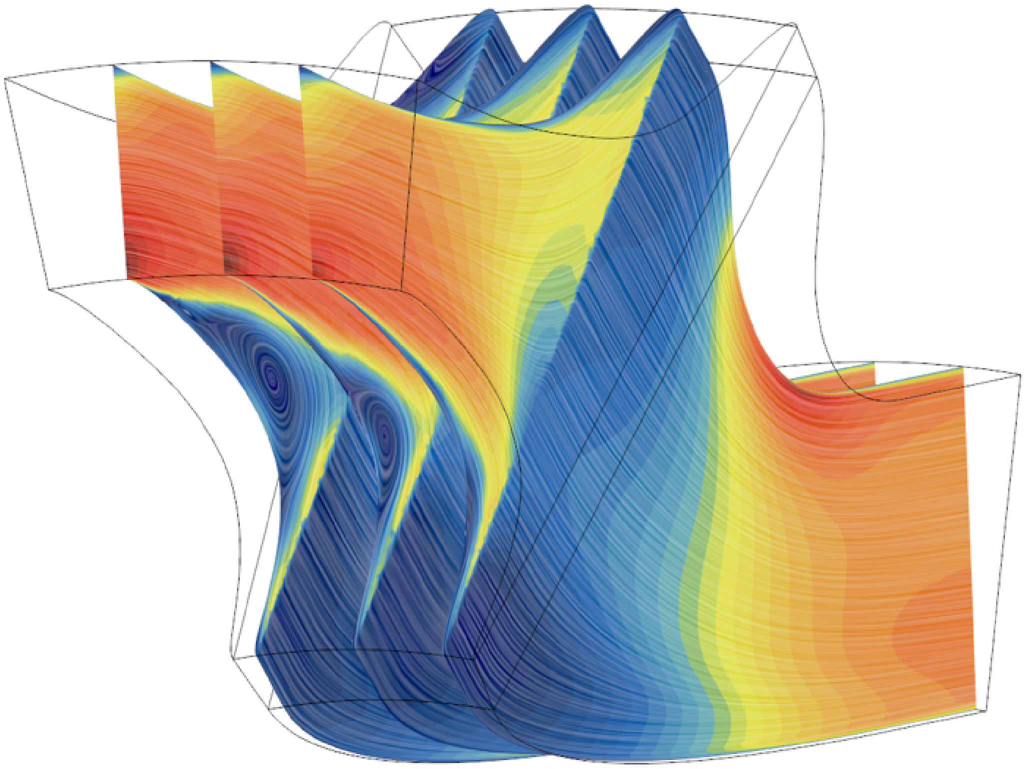

Aerodynamic Evaluation of Intermediate Compressor Ducts with Integrated Heat Exchangers

A study on how three-dimensional flow effects impact the performance of intermediate compressor ducts

ALEXANDER JOHANSSON

DEPARTMENT OF MECHANICS AND MARITIME SCIENCES
CHALMERS UNIVERSITY OF TECHNOLOGY

Gothenburg, Sweden 2026
www.chalmers.se

Master's thesis in Sustainable Energy Systems 2026

Aerodynamic Evaluation of Intermediate Compressor Ducts with Integrated Heat Exchangers

A study on how three-dimensional flow effects impact the performance of intermediate compressor ducts

ALEXANDER JOHANSSON

CHALMERS
UNIVERSITY OF TECHNOLOGY

Department of Mechanics and Maritime Sciences
Division of Fluid Dynamics
Chalmers University of Technology
Gothenburg, Sweden 2026

Aerodynamic Evaluation of Intermediate Compressor Ducts with Integrated Heat Exchangers
A study on how three-dimensional flow effects impact the performance of intermediate compressor ducts
ALEXANDER JOHANSSON

Supervisor: Erik Hasselwander, Department of Mechanics and Maritime Sciences
Examiner: Carlos Xisto, Department of Mechanics and Maritime Sciences

Master's Thesis 2026
Department of Mechanics and Maritime Sciences
Division of Fluid Dynamics
Chalmers University of Technology
SE-412 96 Gothenburg
Telephone +46 31 772 1000

Cover: View of velocity magnitude planes inside a 3D section of an intermediate compressor duct with an integrated heat exchanger.

Typeset in LaTeX
Gothenburg, Sweden 2026

Aerodynamic Evaluation of Intermediate Compressor Ducts with Integrated Heat Exchangers
A study on how three-dimensional flow effects impact the performance of intermediate compressor ducts
ALEXANDER JOHANSSON
Department of Mechanics and Maritime Sciences
Chalmers University of Technology

Abstract

The aviation industry is actively investigating hydrogen as a future aircraft fuel due to its potential to significantly reduce greenhouse gas emissions. One promising application is the use of cryogenic hydrogen for engine heat management through intercooling, where integrated heat exchangers can be placed within intermediate compressor ducts (ICDs) between compressor stages. The aerodynamic performance of such ducts is influenced by complex flow phenomena, including diffuser flow separation, swirl, three-dimensional flow structures, adverse pressure gradients and strong curvature. This thesis investigates the aerodynamic performance of two ICD geometries with integrated heat exchangers using computational fluid dynamics (CFD). The study compares conventional 2D axisymmetric simulations, 2D axisymmetric simulations with swirl modelling, and full 3D simulations in order to evaluate the importance of three-dimensional flow effects. Two diffuser configurations with different lengths and curvatures were analysed using steady-state Reynolds-Averaged Navier-Stokes (RANS) simulations with the $k - \omega$ SST turbulence model. The results show that the shorter and more aggressive diffuser geometry produces around 11% higher total pressure losses than the longer geometry. Full 3D simulations consistently predict higher pressure losses than the corresponding 2D models, indicating that three-dimensional flow effects contribute to additional aerodynamic losses that are not fully captured by axisymmetric approaches. Inlet swirl was found to provide an improvement in diffuser pressure recovery, although its influence on overall pressure losses was limited. The integrated heat exchanger was found to have a significant stabilizing effect on the flow by suppressing diffuser separation, allowing aggressive diffuser geometries to achieve a pressure recovery comparable to less aggressive designs. One important observation is that 2D simulations underpredict both the pressure recovery and total pressure losses by up to 2.5% compared to the performed 3D simulations. The findings suggests that two-dimensional CFD models can provide useful preliminary assessments at a low computational cost, while full three-dimensional simulations are recommended when accurate prediction of flow structures and pressure-loss mechanisms is required.

Keywords: CFD simulation, intermediate compressor duct, integrated heat exchanger, hydrogen aircraft, 3D flow structures.

Acknowledgements

I would like to thank my supervisor, Erik Hasselwander, and my examiner, Carlos Xisto, partly for the opportunity to write this thesis in the first place but also for showing such an interest and providing all the help and feedback you did along the way. I would also like to thank my friends for keeping me company during many late nights of running simulations, and for those of you that helped me work out some of the many challenges with this thesis I am very grateful.

Alexander Johansson, Gothenburg, June 2026

List of Acronyms

Below is the list of acronyms that have been used throughout this thesis listed in alphabetical order:

CC	Combustion Chamber
CFD	Computational Fluid Dynamics
DNS	Direct Numerical Simulation
HEX	Heat Exchanger
HPC	High Pressure Compressor
HPT	High Pressure Turbine
ICD	Intermediate Compressor Duct
LPC	Low Pressure Compressor
LPT	Low Pressure Turbine
RANS	Reynolds-averaged Navier-Stokes

Nomenclature

Below is the nomenclature of indices and variables that have been used throughout this thesis.

Indices

i	Spatial direction, (x,y,z)
j, k	Summation indices
entry	Diffuser entry
exit	Diffuser exit
shroud	Duct shroud surface
hub	Duct hub surface

Variables

r	Radius
r_m	Mean radius
AR	Area ratio
L/D_t	Length to hydraulic diameter ratio
r_t	Throat radius
P, p	Static pressure
p_0	Total pressure
q_{entry}	Inlet dynamic pressure
C_{pr}	Pressure recovery coefficient
ΔP	Pressure drop
dP	HEX inertial resistance scalar
f	Darcy friction factor
L	Pipe length

D_h	Hydraulic diameter
ρ	Fluid density
μ	Dynamic viscosity
V	Average fluid velocity
$\overline{u_i}$	Time-averaged velocity component
u'_i	Instantaneous velocity component
δ_{ij}	Kronecker delta
f_i	Body force
t	Time
x,y,z	Cartesian coordinates
r, θ, z	Cylindrical coordinates
θ	Angular coordinate
z	Axial coordinate
ϕ	HEX tilt angle
$\mathbf{T}$	Inertial resistance tensor
$\mathbf{R}$	Rotational matrix
$\mathbf{T}'$	Corrected inertial resistance tensor

Contents

List of Figures

List of Tables

1
Introduction

1.1 Background

In order to reduce the environmental impact caused by greenhouse gas emissions from commercial aircraft it is becoming more attractive to develop a new generation of turbofan engines that utilize cryogenic hydrogen as fuel. The reasoning behind this is that hydrogen combustion provides a unique opportunity for CO_2 free combustion, in contrast to classic jet fuel which is over 99 % fossil based [1]. A successful hydrogen fueled aircraft engine could therefore solve an important part of existing environmental issues connected to flying. In order to use hydrogen as fuel it must be kept in a liquid state to attain a volumetric energy density that is high enough to comply with storage capabilities of aircraft. This is done by cooling the hydrogen to around 20 Kelvin and storing it in low pressurized cryogenic tanks [2]. However in order to combust the hydrogen fuel in an aircraft engine it must be preheated before reaching the combustion chamber. According to a recent study performed by Chalmers University of Technology and GKN Aerospace [3], the high heat capacity of liquid hydrogen makes it suitable for engine heat management applications. Some examples include compressor intercooling, exhaust gas recuperation and precooling of intake air which could all contribute to reducing the specific fuel consumption of a hydrogen engine design. One proposed way to design an intercooler for a turbofan engine is to place heat exchangers (HEX) in the air ducts between the low and high pressure compressors of the engine. By using intercooling to heat the cryogenic hydrogen the performance of the engine will increase by lowering the inlet temperature of the air entering the combustion chamber [3]. These key opportunities that a hydrogen combustion system provides makes this technology highly interesting to research and refine further.

1.2 State-of-the-art

Diffusers and diffusing ducts have been studied since the 1930s for applications such as aero-engines, wind turbines and ventilation systems. This means that research and experimental studies on different diffuser configurations has already been conducted [4][5] and can be used as a foundation for modern research. However, ducts with integrated heat exchangers is a recent idea that has been proposed as a possible solution to creating intercooling systems for modern hydrogen aircraft engines. Within this research field there is limited research available on the specific aerodynamic design of heat exchanger integration into the diffuser ducts. There are however relevant studies, for example a research study from Chalmers on the optimization of S-duct designs for ICDs with integrated heat exchangers [6]. Regarding specific comparisons of results between two and three dimensional CFD simulations there are studies available for various flow cases but little is aimed at internal flow in diffuser ducts, especially ducts with integrated heat exchangers.

1.3 Purpose

The main objective of this thesis is to investigate the difference between 2D axisymmetric and 3D CFD models applied on intermediate compressor ducts (ICD) containing heat exchangers. This study is only concerned with the aerodynamic performance of the ducts and all heat transfer is excluded. The ICD geometries that will be studied has been provided from ongoing PhD research by Chalmers, with the goal of developing new ICD geometries for use in the Chalmers experimental low pressure compressor rig [7]. These geometries are combined with inlet boundary conditions taken from CFD simulations performed on previous configurations of the same test rig.

The purpose of this study is to learn if three dimensional flow features and swirl which is present in 3D simulations affect the solutions that are obtained compared to 2D simulations where swirl is not included. This is relevant as simulations of diffuser ducts with internal heat exchangers is a field of study with limited research as this type of duct configuration has not had any widespread applications apart from intercooler research for gas turbines [10] and modern research in hydrogen aircraft engines [3]. Results from this study could indicate if two dimensional axisymmetric models are good enough to provide accurate results for this type of simulation or if three dimensional models are necessary to capture important flow features. Knowing this could simplify future work when selecting appropriate CFD models to achieve good results while not wasting computational resources. Due to this integration being new there are many open ended questions that could be answered by this study. The main point of interest in this study is to determine what flow features and effects that are important to capture in order to achieve a high accuracy. Another useful application of this study is as a pre-study to validate new designs for production and use experimentally in the Chalmers low pressure compressor test rig [7]. This could reduce the risk that experimental results differs significantly from previous simulation results while providing additional data for future studies, both experimental and numerical.

2
Theory

This chapters covers the theory that provides the foundation for the analysis of ICDs that is performed in this study. It consists of a section on ICDs, a section on diffusers and a section on the Navier-Stokes equations that are fundamental to the CFD sovler.

2.1 Intermediate Compressor Ducts

The purpose of an ICD is to transport the airflow from the low pressure compressor (LPC) to the high pressure compressor (HPC) system of a turbofan engine. Due to the LPC typically having a larger mean radius compared to the HPC, the ICD is the component that reduces the area of the flow to accommodate this reduction in radius between compressor stages. To minimize the overall length and weight of the aircraft engine these ducts are preferably made as short as possible however, an ICD should also introduce as low losses to the airflow as possible [9]. Figure 2.1 shows the previously mentioned components and the overall layout of a two-spool high bypass turbofan engine.

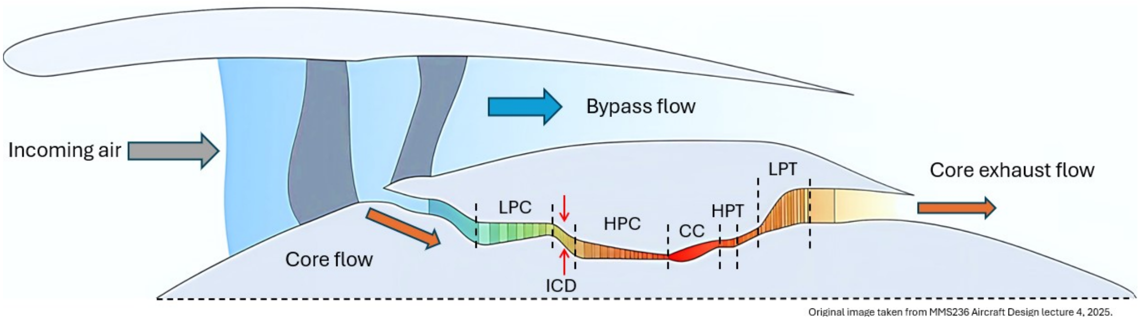

Figure 2.1: Overview of the major components in a two-spool high bypass turbofan engine. The ICD is highlighted with red arrows.

This creates a design problem where aggressive S-shaped duct geometries are needed to fulfill all requirements that are necessary to make a well performing ICD. Figure 2.2 shows an example of an S-duct geometry that was used experimentlly at the Chalmers low pressure compressor test rig. As noted by Britchford et al. [4], flow inside a typical S-duct design becomes complex and is strongly affected by the significant curvature of the duct walls. The combined effects of strong duct curvature and adverse pressure gradients in the streamwise direction, significantly increase the risk of boundary layer separation within the duct. In particular, the pressure redistribution caused by the curvature generates regions of strong adverse pressure gradient along the inner surfaces of the duct, where flow separation is most likely to occur. On the contrary, regions subjected to favourable pressure gradients tend to maintain attached boundary layers and show an increased flow stability.

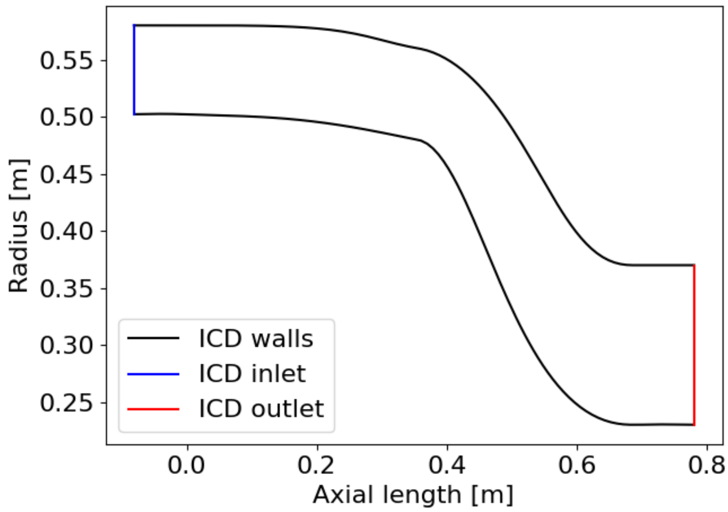

Figure 2.2: Example of S-duct geometry without heat exchanger, taken from a previous setup of the Chalmers low pressure compressor test rig.

2.2 Diffuser ducts

A diffuser is an expanding flow passage designed to reduce fluid velocity and increase static pressure through deceleration of the flow. In aero-engine and gas turbine applications, diffusers are essential components used to convert dynamic pressure into static pressure before the flow enters downstream components such as combustors, compressors, or heat exchangers. The aerodynamic performance of a diffuser duct is strongly influenced by the adverse pressure gradient generated during the deceleration process. As static pressure increases in the streamwise direction, the boundary layer near the wall loses momentum. If this pressure rise becomes too large, local boundary layer separation or diffuser stall may occur which leads to a loss of diffusion and static pressure increase. This will simultaneously introduce recirculation and significant total pressure losses that drastically reduce the diffuser efficiency [5]. Due to this, the diffuser geometry plays a key part in maintaining flow stability while maximizing diffusion of the flow. Some important diffuser parameters are area ratio (AR) and length to mean radius change ($L/\Delta r_m$). These are used to quantify the duct geometries and enable comparison to existing diffuser data.

$$AR = \frac{A_{exit}}{A_{entry}} \tag{2.1}$$

$$L/\Delta r_m = \frac{L}{r_{m,inlet} - r_{m,outlet}} \tag{2.2}$$

In this study the duct length L is defined as a straight line from the mean radius of the diffuser entry to the mean radius of the diffuser exit. One way to quantify the aerodynamic performance of a diffuser is to calculate the pressure recovery coefficient denoted as C_{pr}. This parameter describes how much of the dynamic pressure at the diffuser entry is converted into static pressure over the duct length.

$$C_{pr} = \frac{p_{exit} - p_{entry}}{q_{entry}} \tag{2.3}$$

Generally for a classic diffuser duct configuration, a diffuser is more likely to experience flow separation when $(L/\Delta r_m)$ is low and (AR) is high, which is why longer diffusers with less aggressive curvature produce higher values of C_{pr} compared to short diffusers with large area ratios.

According to experimental evaluation of various diffuser designs it has been concluded that a moderate amount of inlet swirl might help diffusion and improve diffuser performance. However an important observation is that diffusers that are close to experiencing stall are highly sensitive to inlet swirl and in those cases swirl might negatively affect the overall performance of the diffuser [5].

When integrating a HEX into a diffuser duct the flow behaviour of the diffuser is affected by the pressure field redistribution the HEX causes. Inside of the HEX the flow is straightened and any swirl is either removed or greatly reduced by the internal structure of the HEX. However in addition to this, the presence of the HEX in the flowpath causes the pressure distribution upstream of the HEX to change. This effect has shown a potential to reduce flow separation immediately upstream of the HEX [8]. This effect enables diffuser designs with stronger curvature, shorter lengths and/or higher area ratios to perform comparably to conventional designs, despite the geometry being too aggressive to effectively be used in a clean duct configuration.

2.3 Navier-Stokes equations

The governing equations for fluid motion used by the CFD solver are called the Navier-Stokes equations, these are what the CFD solver uses to numerically solve any flow field that is being simulated. The first equation is called the continuity equation, where ρ denotes the fluid density and v the fluid velocity in a direction x.

$$\frac{d\rho}{dt} + \rho\frac{\partial v_i}{\partial x_i} = 0 \tag{2.4}$$

The second equation is called the the momentum equation where P denotes pressure, μ dynamic viscosity and ρf_i body forces. Examples of body forces are gravity and centrifugal forces.

$$\rho\frac{dv_i}{dt} = -\frac{\partial P}{\partial x_i} + \frac{\partial}{\partial x_j}\left(\mu\left(\frac{\partial v_i}{\partial x_j} + \frac{\partial v_j}{\partial x_i}\right) - \frac{2}{3}\mu\frac{\partial v_k}{\partial x_k}\delta_{ij}\right) + \rho f_i \tag{2.5}$$

2.3.1 Reynolds averaged Navier-Stokes

Solving the Navier-Stokes equations directly is a method called direct numerical simulation (DNS). This method quickly gets numerically impractical as simulation meshes increase in cell count and as flow velocities increase. This makes DNS a computationally expensive and time-consuming method for solving most CFD problems. A common method to reduce the computational cost of simulations is to instead solve the Reynolds-Averaged Navier-Stokes equations (RANS). The key difference from the standard Navier-Stokes is that in RANS the velocity terms are split into a time averaged part and a fluctuating part. This mathematical approach is called Reynolds-decomposition and is described in equation 2.6.

$$u_i = \overline{u_i} + u_i' \tag{2.6}$$

By implementing the Reynolds-decomposition in the Navier-Stokes equations the RANS equations 2.7 and 2.8 are formulated.

$$\frac{\partial \overline{u}_i}{\partial x_i} = 0 \tag{2.7}$$

$$\rho\,\overline{u}_j \frac{\partial \overline{u}_i}{\partial x_j} = \frac{\partial}{\partial x_j}\left[-\overline{p}\delta_{ij} + \mu\left(\frac{\partial \overline{u}_i}{\partial x_j} + \frac{\partial \overline{u}_j}{\partial x_i}\right) - \rho\overline{u_i' u_j'}\right] \tag{2.8}$$

However, formulating the RANS equations using this method creates a mathematical problem known as a closure problem. To resolve the closure problem the RANS equations are complemented by a turbulence model that solves the non-linear Reynolds-stress term $\rho\overline{u_i' u_j'}$. The model used for this study is the $k-\omega$ Shear Stress Transport (SST) turbulence model which is one of the most commonly employed for various types of engineering studies.

2.3.2 $k - \omega$ SST

The $k-\omega$ SST model is among the most widely used two-equation turbulence models in engineering CFD applications due to its robustness and ability to accurately predict a wide range of turbulent flows. The $k-\omega$ SST model combines the strengths of the standard $k-\omega$ and $k-\epsilon$ models through a blending function. In the near-wall region the model behaves as a $k-\omega$ model, which provides accurate predictions of boundary-layer development and flow separation. Further away from the wall the formulation gradually transitions towards a $k-\epsilon$-type model which performs better in the free stream, away from walls and outside boundary layers. This contributes to a turbulence model that is suitable for the flow conditions investigated in this thesis, as adverse pressure gradients and swirl are always present within the diffuser ducts and flow separation may occur in some cases. The $k-\omega$ SST model is generally considered to produce accurate predictions in flow regions with moderate curvature. However, the studied duct geometries contains some regions where wall curvature is quite strong, especially in the short geometry. For this application using the $k-\omega$ SST model with curvature correction could possibly provide better simulation accuracy.

3
Method

This chapter explains the methodology used to create a numerical model for each of the provided ICD geometries. This includes selection of physics models in STAR-CCM, implementation of boundary conditions from previous 3D-RANS simulations, heat exchanger modeling and creation of computational meshes for each simulation.

3.1 Geometries

The two ICD geometries that were used for simulations in this thesis were provided from ongoing PhD research by Chalmers on developing a new ICD for use in the experimental low pressure compressor rig at Chalmers. These geometries were referred to as the long and short geometry, respectively. The difference between the geometries lie in the length and shape of the diffusing duct, as the HEX section and contracting duct are identical for both ICDs. The ICDs studied in this thesis differ significantly from the traditional S-duct design by the addition of an integrated HEX in the middle of the ICD in combination with an unusually high area ratio. These ducts are comprised of three main parts, a diffusing duct, a heat exchanger and a contracting duct which are showed in figure 3.1.

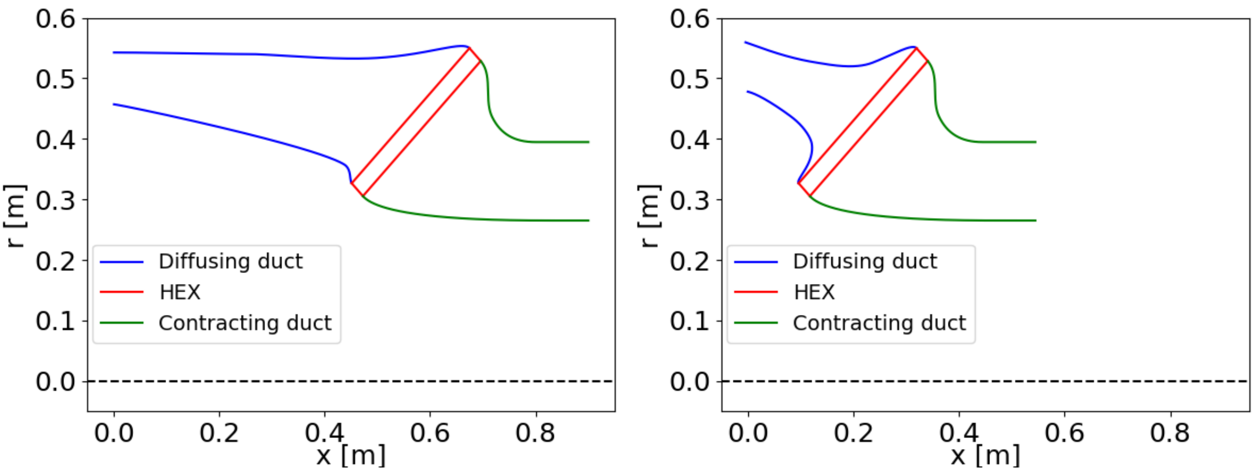

(a) Long ICD geometry. **(b)** Short ICD geometry.

Figure 3.1: Cross section views of both ICD geometries, with the engine symmetry line marked with black dashed line.

The diffusing duct acts as the inlet section of the ICD as this is where the airflow coming from the upstream compressor stage enters the ICD. The purpose of this section is to slow down incoming air and recover as much pressure as possible in the fluid, while maintaining a uniform flow. The HEX section introduces a pressure drop to the airflow which is modeled as a porous region with an inertial resistance. The HEX section will also help align the flow by not allowing any flow in the radial direction at the cost of some pressure drop. Lastly the contracting duct reduces the flow area, lowering the pressure and accelerating the fluid towards the HPC inlet. The geometric parameters for each ICD, explained in chapter 2.2 can be seen in table 3.1.

Table 3.1: Geometric parameters for long and short diffuser configurations.

Geometry	**AR**	$\mathbf{L/\Delta r_m}$
Long	3.69	9.16
Short	3.85	3.47

3.2 Physics models

In this study both the 2D-axisymmetric and 3D models available in StarCCM are used. The 2D-axisymmetric model is used in standard configuration and with axisymmetric swirl enabled. The optional axisymmetric swirl model uses a regular 2D-mesh but solves the momentum equation for the Z-direction which represents the swirl motion present in the flow. This allows for a simple analysis of three-dimensional flow effects at a significantly lower cost compared to a full 3D simulation, at the cost of solution accuracy. All simulations performed are done using a steady state solver since the duct flow is expected to reach a sufficiently steady state that does not require the use of an unsteady solver. This assumption is based on the fact that the inlet and outlet conditions are constant and that the duct geometry does not change during simulation, there are also no components with a periodic behaviour such as rotating compressor blades present. No large separation that could cause vortex formation in a recirculation zone is expected since the HEX should help stabilize the flow [8], which means that significant large scale unsteady physics is not expected to appear in the duct. Previous numerical studies of diffuser ducts have shown that RANS captures the flow features of a diffuser duct with acceptable accuracy despite being a simple model. The choice of a steady state RANS solver also reduces computational costs significantly compared to using a transient solver.

A coupled CFD solver with second-order discretization was selected, due to its capability to resolve swirling flows with potential recirculation better compared to a segregated solver. The coupled solver also typically handles strong pressure gradients more efficiently than a segregated solver which often leads to faster converging simulations and should provide better numerical accuracy for the present conditions. A constant-density incompressible flow model was employed, as the investigated flow conditions correspond to Mach numbers in the 0.10 - 0.15 range, where compressibility effects are considered negligible. As previously mentioned in section 2.3.2 the k-ω SST turbulence model was selected due to its wide range of applications including internal flows involving adverse pressure gradients, separation, and swirling flow structures. This makes it well suited for the flow conditions investigated in this study [11]. Table 3.2 contains a complete list of the physics models used in StarCCM.

Table 3.2: Summary of used StarCCM physics models.

Physical aspect	**Model**
Fluid type	Gas
Solver	Coupled flow
Geometry	Axisymmetric (2D) / 3D
Equation of state	Constant density
Time dependence	Steady
Flow structure	Turbulent flow
Turbulence model	k-ω SST

3.3 Boundary conditions

The inlet of the duct was defined as a stagnation inlet with a set of boundary conditions that match the experimental compressor rig that the studied geometries are intended to be used in. The inlet boundary conditions for the performed simulations were provided from a previous three-dimensional RANS study of two different ICD configurations from the same compressor test rig [7]. This data contained a set of radial profiles for total pressure, total temperature, turbulent kinetic energy, specific dissipation rate and velocity components which correspond to each of the two studied geometries. This data was used both for the 2D and 3D cases without modification. The inlet velocity profiles are shown in figure 3.2, while the temperature and pressure profiles can be found in Appendix A.

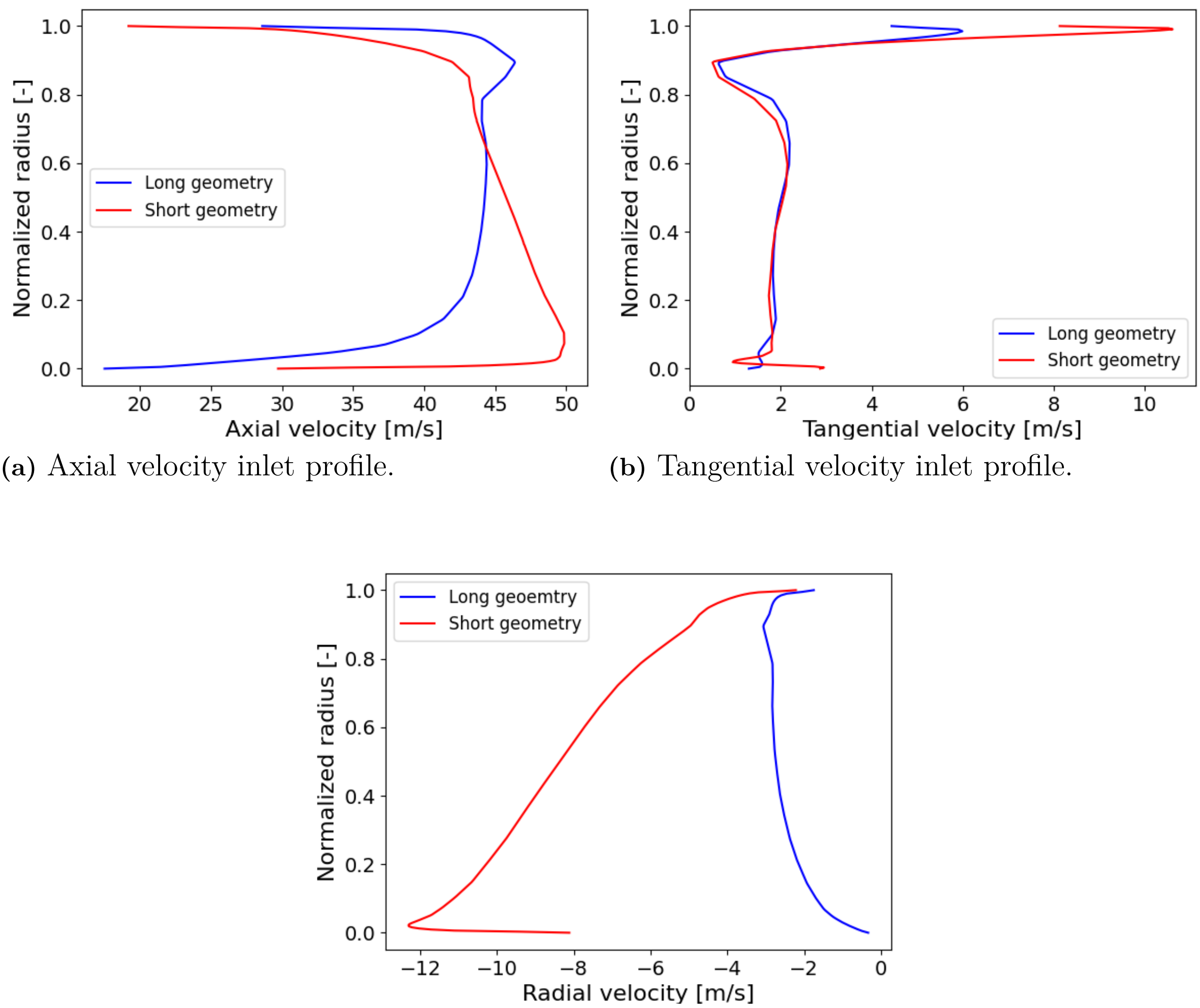

(a) Axial velocity inlet profile.

(b) Tangential velocity inlet profile.

(c) Radial velocity inlet profile.

Figure 3.2: Radial inlet profiles for axial, tangential and radial velocities. The tangential velocity defines the swirl component of the flow.

The average values of each radial inlet profile are summarized in tables 3.3 and 3.4. For both geometries the inlet conditions are similar however, the short duct notably has higher velocities in all directions, especially the swirl velocity which is roughly three times higher compared to the long duct.

Table 3.3: Radially averaged inlet boundary conditions for long duct.

Parameter	**Value**
Total pressure	98877.4 Pa
Total temperature	291.6 K
Axial velocity	42.54 m/s
Radial velocity	-2.47 m/s
Tangential velocity	1.99 m/s
Mach number	0.12

Table 3.4: Radially averaged inlet boundary conditions for short duct.

Parameter	**Value**
Total pressure	98891.1 Pa
Total temperature	291.6 K
Axial velocity	45.05 m/s
Radial velocity	-8.19 m/s
Tangential velocity	2.06 m/s
Mach number	0.13

The outlet of the duct was defined as a pressure outlet with a target mass flow rate. This means that the outlet pressure is adjusted every iteration to make the simulation reach a selected mass flow target value. This value differed between the 2D and 3D cases, since the mass flow must be proportional to the flow area of the geometry. The mass flow used in the simulation of the experimental rig that provided the inlet boundary conditions is 13 kg/s. In 3D the total massflow of 13 kg/s was divided by 20 to represent an 18 degree section cut of the full 360 degree geometry.

3.4 Heat exchanger modeling

To accurately capture the physical impact a finned HEX would have on the airflow through the ICD geometries, the HEX must be modeled in the simulation software. This was done by numerically representing the HEX section as a porous media. It has previously been showed that porous media modeling is an effective way to study the effects of flow through heat exchangers and connecting ducts, at a low computational cost [11]. There are two physical aspects of a HEX that are relevant to this study, the first being the pressure drop that occurs as the flow moves through the HEX. This value is controlled by employing a porous heat exchanger model to mimic a real HEX geometry being placed in the flowpath of the air. The pressure drop of a HEX describes how much flow losses are incurred by the obstruction of the fluid and will vary depending on the design of the heat exchanger and scales quadratically with the velocity of the entering fluid, according to the Darcy-Weisbach equation,

$$\Delta P = f \frac{L}{D_h} \frac{\rho V^2}{2} \tag{3.1}$$

which uses the following notation:

$$\begin{aligned}\Delta P &= \text{pressure drop}\\ f &= \text{Darcy friction factor}\\ L &= \text{pipe length}\\ D_h &= \text{hydraulic diameter}\\ \rho &= \text{fluid density}\\ V &= \text{average fluid velocity.}\end{aligned}$$

The second aspect is the possible directions the flow can move in while passing through the HEX model. In this case a finned heat exchanger is what the porous media will be based on. The fins extend along the axial and tangential directions of the HEX and are spaced radially to create a geometry similar to what can be seen in figure 3.3. This means that the flow can move relatively easily in the axial and tangential directions while being completely prohibited from moving radially inside the heat exchanger region. This can be seen in figure 3.6 as the flow being restricted in the local Y direction but free to move along the local X and Z-axes.

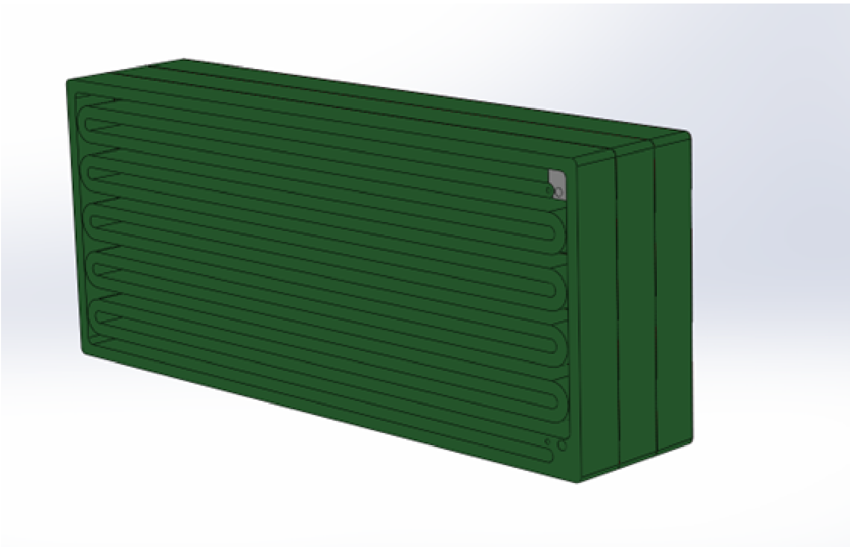

Figure 3.3: Example of finned HEX that is similar to what will be used experimentally at the Chalmers low pressure compressor test rig [7].

3.4.1 Measurement definitions

To calculate flow parameters in different sections of the ICD, the geometry was divided by measuring planes that can be seen in figure 3.4 as black dashed lines within the duct geometry. The area between planes 1 and 2 is the diffuser, between planes 2 and 3 the HEX and between 3 and 4 the contracting duct, these definitions will be used for all presented calculations. The reason for defining these planes instead of using the natural borders of the geometry is that the flow field tends to become slightly irregular at the HEX entry and exit, which can be seen in figure 3.5. To avoid getting inconsistent measurement data planes 2 and 3 were offset from the actual HEX geometry by 3mm, which places them just outside the non uniform flow area at the HEX boundary.

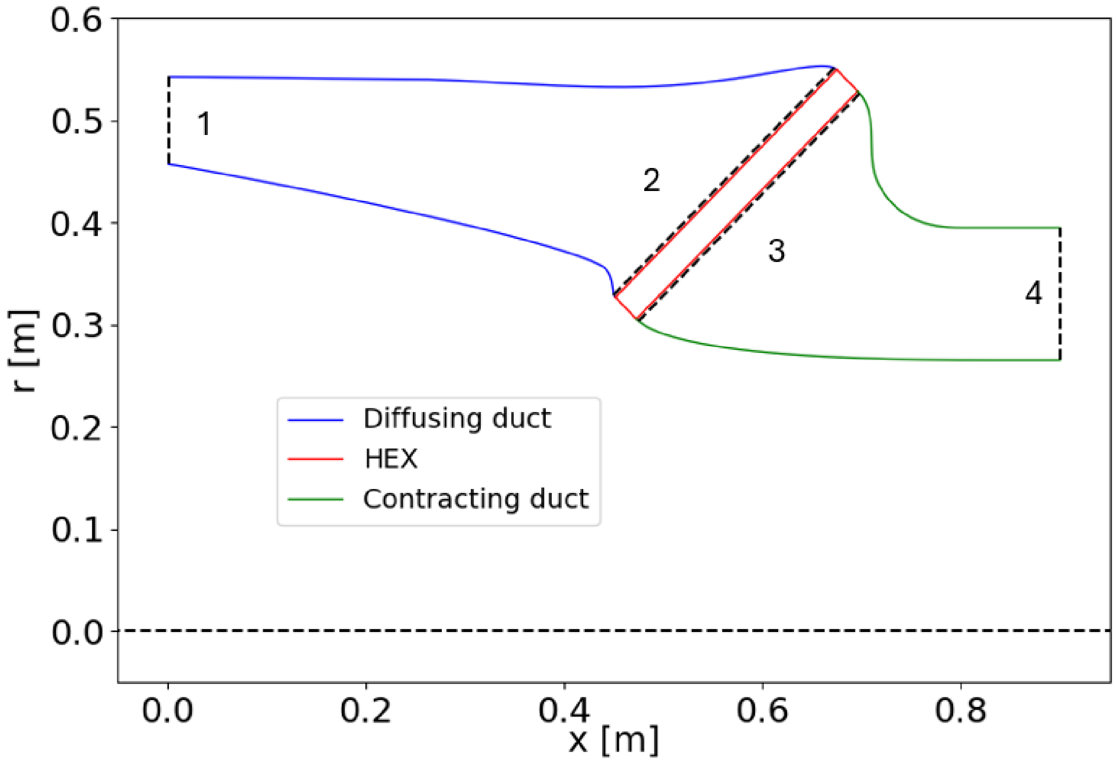

Figure 3.4: Definition of measuring planes for each ICD section.

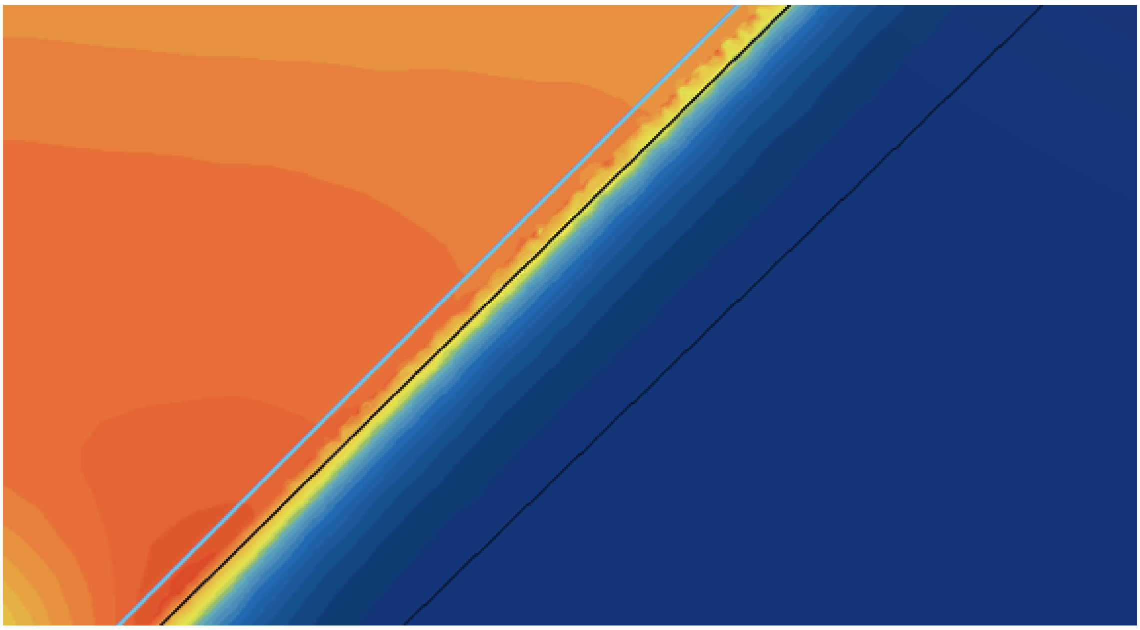

Figure 3.5: Zoomed image of tangential velocity field at the HEX entry. The black lines indicate the HEX geometry and the blue line indicates the offset measuring plane at the HEX entry.

3.4.2 2D HEX model

To define the porous media model in StarCCM, inertial resistance tensors were used to represent the momentum loss experienced by the fluid as it flows through the porous region. This allows the CFD-solver to reproduce a pressure-drop behavior similar to that of a full geometric model. These tensors differ slightly between 2D and 3D simulations since the coordinate systems of these two geometries are defined differently. In 2D an orthotropic tensor is used to describe the inertial resistance through the porous region. The orthotropic tensor has a unique value in each principal direction, so for a 2D simulation this would be along the X and Y-axes respectively. Since the HEX region in the duct geometries used in this study are inclined at $-45°$ around the Z-axis, the inertial resistances have to reflect this. This is done by assigning a new local coordinate system that is rotated by $-45°$ around the Z-axis. Using this local coordinate system which can be seen in figure 3.6, the inertial resistances can easily be assigned in the local X and Y-directions for the HEX region.

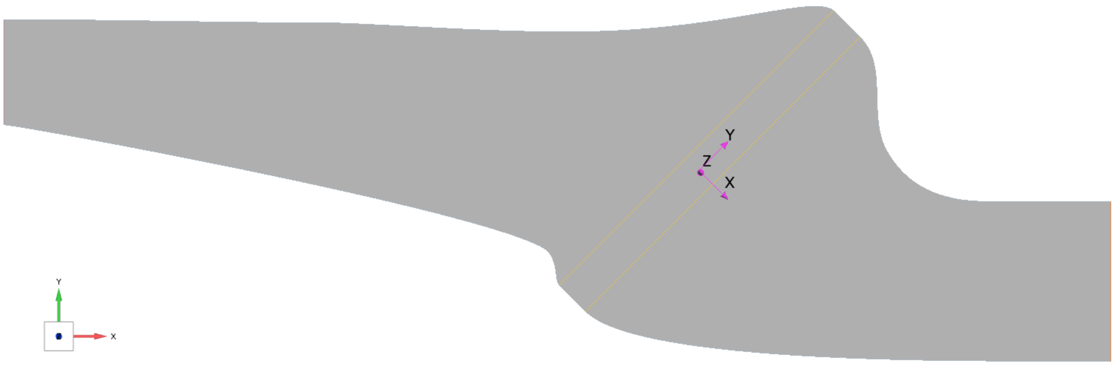

Figure 3.6: Image of the long duct geometry in 2D with local coordinate sytem for the HEX displayed in purple.

3.4.3 3D HEX model

In a 3D geometry the inertial resistance will have to be assigned using a cylindrical coordinate system, since the real 3D geometry is rotationally symmetric around the centerline of an aircraft engine. To achieve this a new local cylindrical coordinate system on the form (r, θ, z) is introduced which has its origin in the origin of the global coordinate system of the simulation, which is in [0,0,0]. The inertial resistance in the 3D simulations is described by an anisotropic tensor which will be called $\mathbf{T}$.

$$\mathbf{T} = \begin{pmatrix} T_{rr} & T_{r\theta} & T_{rz} \\ T_{\theta r} & T_{\theta\theta} & T_{\theta z} \\ T_{zr} & T_{z\theta} & T_{zz} \end{pmatrix} \tag{3.2}$$

In order to get the correct inertial resistances related to the geometry of the HEX region the tensor $\mathbf{T}$ has to be rotated to match the $-45°$ angle that the HEX is inclined. This can be done using the matrix multiplication in equation 3.3.

$$\mathbf{T'} = \mathbf{R}\,\mathbf{T}\,\mathbf{R^T} \tag{3.3}$$

$\mathbf{T'}$ represents $\mathbf{T}$ when projected onto the $-45°$ plane of the HEX and $\mathbf{R}$ is the rotational matrix which contains the angles for each tensor component of $\mathbf{T}$ when $\phi = -45°$.

$$\mathbf{R} = \begin{pmatrix} \cos\phi & 0 & \sin\phi \\ 0 & 1 & 0 \\ -\sin\phi & 0 & \cos\phi \end{pmatrix} = \begin{pmatrix} \frac{\sqrt{2}}{2} & 0 & -\frac{\sqrt{2}}{2} \\ 0 & 1 & 0 \\ \frac{\sqrt{2}}{2} & 0 & \frac{\sqrt{2}}{2} \end{pmatrix} \tag{3.4}$$

$$\mathbf{T} = \begin{pmatrix} 1000 & 0 & 0 \\ 0 & 1 & 0 \\ 0 & 0 & 1 \end{pmatrix}$$

By assigning resistances in the cylindrical coordinate system the tensor for inertial resistance can be calculated. Since the model for the HEX is based on a finned heat exchanger as explained earlier in the chapter, the inertial resistance in the radial direction is defined to be a factor of 1000 larger compared to the other two directions. The purpose of this is to represent the physical blockage that the fins in the HEX would cause in a full geometric model.

By performing the matrix multiplication described in equations 3.3 and 3.5 the inertial resistance tensor that was used for the 3D simulations is obtained. Each term of the tensor is then scaled by a scalar called dP to adjust the pressure drop over the HEX section in the simulations. This ensures that the inertial resistance terms maintain the correct relation to each other while the pressure drop is easily adjustable for different simulation setups.

$$\begin{pmatrix} T'_{rr} & T'_{r\theta} & T'_{rz} \\ T'_{\theta r} & T'_{\theta\theta} & T'_{\theta z} \\ T'_{zr} & T'_{z\theta} & T'_{zz} \end{pmatrix} = \begin{pmatrix} \cos\phi & 0 & \sin\phi \\ 0 & 1 & 0 \\ -\sin\phi & 0 & \cos\phi \end{pmatrix} \begin{pmatrix} 1000 & 0 & 0 \\ 0 & 1 & 0 \\ 0 & 0 & 1 \end{pmatrix} \begin{pmatrix} \cos\phi & 0 & -\sin\phi \\ 0 & 1 & 0 \\ \sin\phi & 0 & \cos\phi \end{pmatrix} \tag{3.5}$$

$$\mathbf{T'} = \begin{pmatrix} 500.5 & 0 & 499.5 \\ 0 & 1 & 0 \\ 499.5 & 0 & 500.5 \end{pmatrix} \tag{3.6}$$

3.5 Numerical Mesh

3.5.1 2D mesh

The mesh for the 2D simulation cases consists of a polygonal mesher with prism layers on all walls which are used to accurately resolve near wall flow. The cell face target size was set to be equal to 50 % of the selected base size of the mesh with a surface growth rate of 1.3. The selected prism layer settings presented in table 3.5 defined the base mesh. In order to reduce computational cost of the 3D simulations the mesh for both geometries used a coarser mesh setting for the contracting duct, which was defined by a target surface size equal to 300 % of the base size. The prism layers in the contracting duct and HEX region was also modified by halving the total thickness of the prism layer compared to the inlet region. Since the flow in the contracting section of the duct no longer faces an adverse pressure gradient and the geometry is contracting rather than expanding, the boundary layer thickness becomes smaller which makes a reduction in prism layer thickness a reasonable adjustment. For both meshes wall y+ was kept below one across all walls to ensure that the near wall flow was resolved sufficiently. When performing a mesh independence study the base size of the mesh was modified to adjust the cell count of each mesh to control the convergence of the solution.

Table 3.5: Prism Layer Parameters used for 2D and 3D meshes.

Prism Layer Parameters	**Value**
Number of Prism Layers	25
Prism Layer Stretching	1.3
Prism Layer Reduction Percentage	0
Prism Layer Total Thickness	0.003 m
Concave Angle Limit	0.0 deg
Convex Angle Limit	360.0 deg
Near Core Layer Aspect Ratio	0.5
Gap Fill Percentage	25.0
Minimum Thickness Percentage	10.0
Boundary March Angle	50.0 deg

3.5.2 3D mesh

The mesh for the 3D simulation cases consists of a polyhedral mesher with post mesh optimization enables. It also uses prism layer meshing on all walls like in the 2D cases. This combination is strongly recommended for volume meshing of internal flows as the polyhedral mesh is quite efficient at generating well structured conformal meshes. It also provides good accuracy of regions with strong gradients thanks to the structure of the polyhedrals themselves [12]. Since each cell typically will have up around ten or more neigbouring cells the risk of problems like numerical diffusion is greatly reduced compared to an orthogonal mesh for example. This means that the polyhedral mesh is likely to capture important areas of the flow accurately without requiring as careful refinement and quality control as other mesh types. When generating the 3D mesh an optional function in StarCCM called surface remesher was used, with the function automatic surface repair enabled. This feature improves the overall quality of the mesh by the increasing mesh conformity over all parts of the geometry. The mesh itself uses a volume growth rate of 1.1 and a target surface size equal to 25 % of the mesh base size. Just like the 2D meshes the 3D meshes use a coarser mesh setting for the contracting duct and HEX sections to reduce computational cost by saving cells in the regions that are less sensitive to this study.

3.5.3 Mesh convergence

To ensure that each computational mesh was sufficiently refined, a mesh convergence study was performed. Each mesh started with a cell count of 50 000 cells for the 2D cases, 500 000 cells for the short geometry in 3D and 1 000 000 cells for the long geometry in 3D. The mesh resolution was progressively increased by systematically reducing the base cell size, resulting in an approximate doubling of the total cell count between successive refinement levels. This process was repeated until each solution showed negligible sensitivity to further mesh refinement. Mesh independence was assessed by comparing the total pressure drop across the entire duct for each mesh refinement level. The pressure drop values were normalized with respect to the finest mesh in each refinement series in order to quantify the relative deviation.

4

Results

This chapter presents the results and discussion for the ICD simulations, the diffuser performance and the flow stabilizing effect of the heat exchanger.

4.1 Simulation convergence

4.1.1 Mesh convergence

The mesh convergence study explained in section 3.5.3 resulted in mesh sizes for the 2D meshes of 1 500 000 and 800 000 cells for the long and short geometries respectively. The convergence of the mesh sizes for the 2D meshes can be seen in figure 4.1 below. For the 3D simulations the final mesh sizes were 8 million cells for the long and 4 million cells for the short geometry. For the mesh study of the 3D simulations it is important to note that the mesh for the long geometry does not appear to graphically converge, which is showed in figure 4.2a. However the difference between the final two meshes only represents an increase of the total pressure drop over the ICD by 0.2 %, when mesh size was increased from 4 to 8 million cells. This difference was considered sufficiently converged and no further refinements were made.

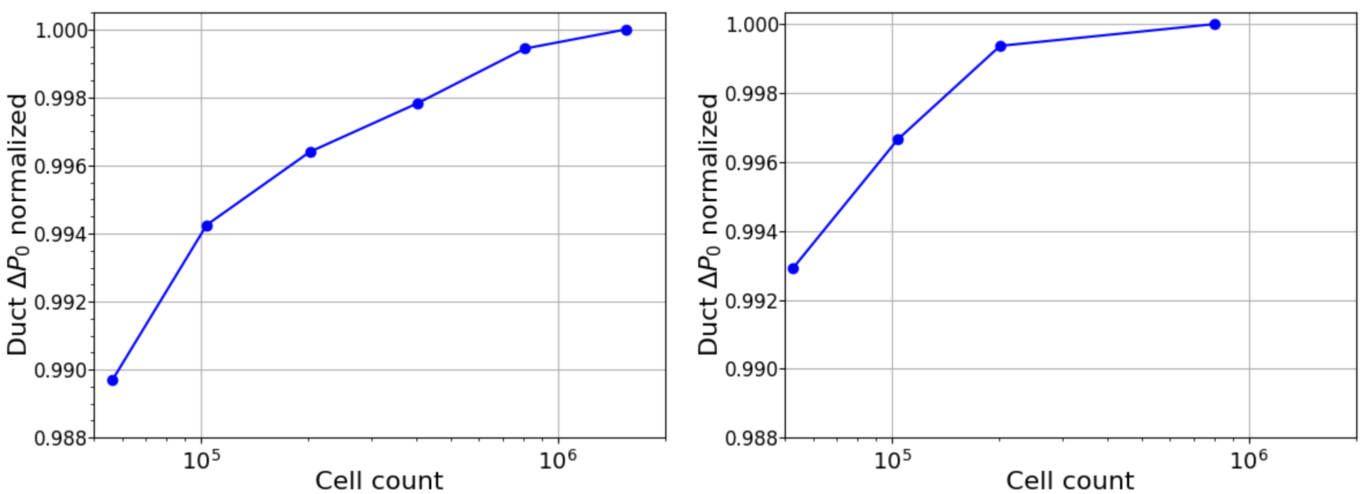

(a) 2D mesh convergence, long ICD geometry. **(b)** 2D mesh convergence, short ICD geometry.

Figure 4.1: Mesh convergence study of 2D meshes.

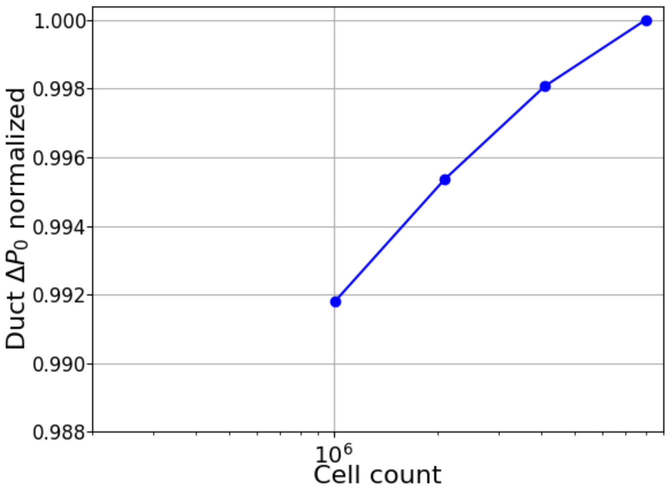

(a) 3D mesh convergence, long ICD geometry.

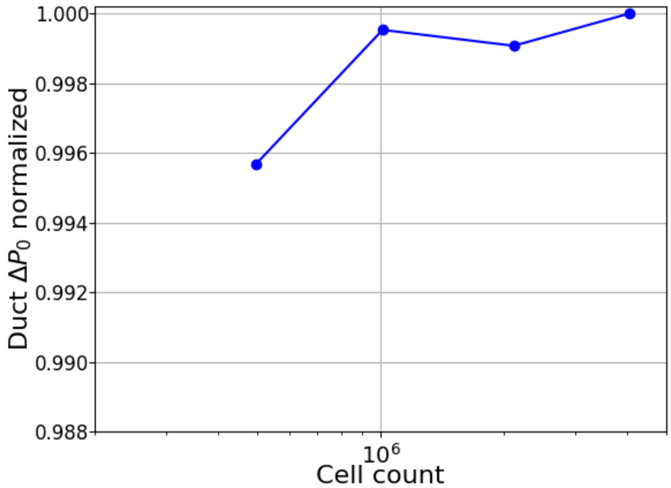

(b) 3D mesh convergence, short ICD geometry.

Figure 4.2: Mesh convergence study of 3D meshes.

4.1.2 Solution convergence

For each simulated case, solution convergence was assessed by monitoring a combination of solver residuals and flow quantities. Particular attention was given to the near-wall flow of the diffuser duct and the total pressure drop over the entire ICD. The surface average of the wall shear stress on both the diffuser hub and shroud surfaces was monitored to ensure that the boundary layer in the diffuser had reached a converged state. In all cases the wall shear stress exhibited a large initial drop that later converged to a constant value for each respective term, indicating that the near-wall flow had stabilized and that the boundary layer development had reached a steady state solution. The total pressure drop over the entire ICD displayed similar behaviour to the wall shear stress monitor, as showed in the convergence data from figure 4.3. For all the simulation setups these control variables reached a steady solution, both for 2D and 3D despite different behaviour of the solver residuals for each case.

The convergence behaviour of the solver residuals differed between the 2D and 3D simulations. In the 3D cases, all residuals decayed smoothly and the simulations were terminated after approximately 400 iterations, once the largest residual had decreased by six orders of magnitude. At this stage, all monitored flow quantities had reached steady values and showed no significant variation with further iterations, indicating that the solution was sufficiently converged. In the 2D simulations, the continuity and z-momentum residuals ceased to decrease after approximately three to four orders of magnitude and exhibited small oscillations thereafter. However, all monitored flow variables had stabilized and remained effectively constant for several hundred iterations. Consequently, each of 2D simulations were stopped after 800 iterations and considered converged despite the residual plateau.

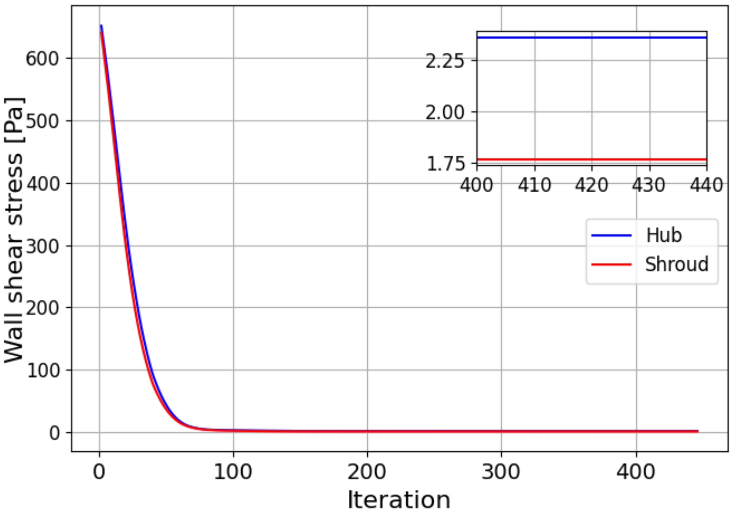

(a) Diffuser wall shear stresses.

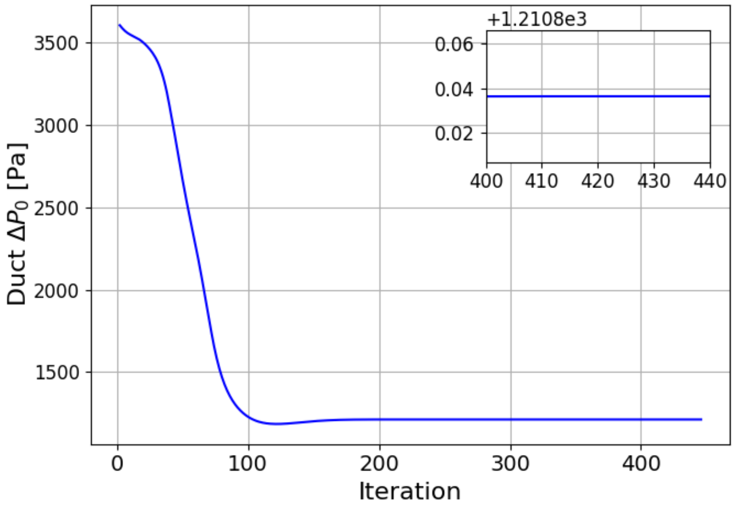

(b) ICD total pressure drop.

Figure 4.3: Solution convergence history of wall shear stresses and total pressure drop for short geometry 3D simulation.

4.2 Overview of Simulated Cases

The data presented in table 4.1 shows the measured total pressure drop over the ICD for the three different simulation setups that were made for each respective geometry. For all simulation models the short ICD geometry resulted in higher total pressure losses compared to the long ICD geometry. This indicates that the short ICD incurs a larger aerodynamic penalty on the flow, however this could partially be attributed to the fact that the inlet conditions for the short ICD had slightly higher velocities in all three directions. This should contribute to some increase in losses over the HEX as the pressure drop increases with the square of the velocity according to the Darcy-Weisbach equation, 3.1. The total pressure drop data also shows that the 3D simulations have consistently higher losses than the 2D simulations, which indicates that three-dimensional effects cause additional losses that are not captured by the 2D models.

Table 4.1: Absolute total pressure drop over entire ICD.

Case	ΔP_0 **[Pa]**	ΔP_0 [%]
Long 2D	1080.71	1.093
Long 2D swirl	1085.38	1.098
Long 3D	1093.92	1.106
Short 2D	1188.34	1.201
Short 2D swirl	1202.29	1.215
Short 3D	1210.8	1.224

4.3 Comparison Between 2D and 3D Simulations

The following two sections present the pressure drops for each simulation setup in addition to the decay of the swirl present in the flow.

4.3.1 Pressure drop distribution

When observing the total pressure drops of the diffuser and HEX sections for the long geometry, there is an interesting difference between the 2D and 3D case. When introducing the swirl in the 3D simulation the losses over the diffuser slightly increase compared to the 2D simulation, while the HEX losses decrease. This indicates that more diffusion is taking place in the diffuser and this results in a lower flow velocity at the entry of the HEX. Looking at the Darcy pressure drop equation 3.1, it is reasonable that the increased diffusion prior to the HEX lowers the losses caused by the HEX itself. When summarizing the loss terms in the diffuser-HEX system for each case it can be seen that this redistribution of the loss terms due to increased diffusion in the inlet duct leads to a reduction of total pressure losses corresponding to 1.22% of the inlet dynamic pressure. This means that the diffuser and HEX section combined, appears to perform marginally better in the 3D case where the presence of could inlet swirl help diffuse the flow more effectively than what is seen in the two-dimensional flow.
Analyzing the short duct geometry reveals a similar trend however the differences are significantly smaller between the different simulation setups. The 3D case experiences a reduction of total pressure loss corresponding to 0.23% of the inlet dynamic pressure, this is roughly five times less than the reduction seen in the long ICD geometry. This suggests that the three-dimensional effects of the inlet swirl could be improving diffusion and thus the overall efficiency of the diffuser-HEX system. However these differences are quite small and could be sensitive to small changes in both inlet conditions and mesh refinement.

Table 4.2: Total pressure drop over each duct section, normalized to the inlet dynamic pressure of each respective simulation setup.

Case	Diffuser duct [%]	HEX [%]	Outlet duct [%]
Long 2D	1.90	101.84	1.67
Long 2D swirl	1.88	102.34	1.64
Long 3D	2.04	100.48	4.22
Short 2D	1.01	95.97	1.35
Short 2D swirl	1.20	96.80	1.42
Short 3D	1.22	95.53	3.46

According to the data presented in table 4.2 the 3D cases for both ICD geometries show an increase of losses in the outlet duct by a factor of 2.5 compared to both the 2D models used. This increase was not expected and despite investigating the flow through the outlet duct no definitive reason for this increase was found. The wall shear stress distribution along the hub and shroud walls were found to be practically identical between 2D and 3D models and the average wall shear stress on these surfaces only varied by a few percent. Considering the fact that the circumferential velocity is essentially completely dissipated after the HEX as seen in figure 4.4, the inlet swirl in the 3D simulation is unlikely to directly contribute to this increase in outlet duct losses. Although an increase of 2.5 times is a large relative change, the actual pressure loss only corresponds to 1% of the total pressure loss in 2D and around 3% in the 3D simulations. Since this difference is quite small the increase in losses could possibly depend on differences in mesh resolution or numerical differences between the 2D and 3D CFD models.

4.3.2 Swirl decay

By comparing the swirl velocity through contour plots of the 2D axisymmetric-swirl model, figure 4.4a and the full 3D model, figure 4.4b it becomes clear that the swirl does not decay when passing through the HEX region in the 2D simulation. This is due to the way the inertial resistances are modeled in each simulation setup. In the 2D simulations the HEX inertial resistance only contains terms for the axial and radial directions since it is applied to a two-dimensional mesh. In the 3D simulations a three-dimensional tensor is used to apply the inertial resistance to the HEX region, which causes the swirl to decay in the HEX. This difference does not appear to directly impact the simulation results for pressure drop, however it could prove very important if there are downstream components that are affected by swirling flow. When analyzing how a HEX interacts with the flow through and ICD, this lack of inertial resistance becomes a significant simplification that generally makes the 2D-axisymmetric swirl model less accurate for this type of analysis. To make the 2D-axisymmetric swirl model more viable when analyzing flow through heat exchangers this neglected loss term could be addressed by introducing a specific loss term through a field function that calculates pressure drop based on the circumferential velocity of the flow.

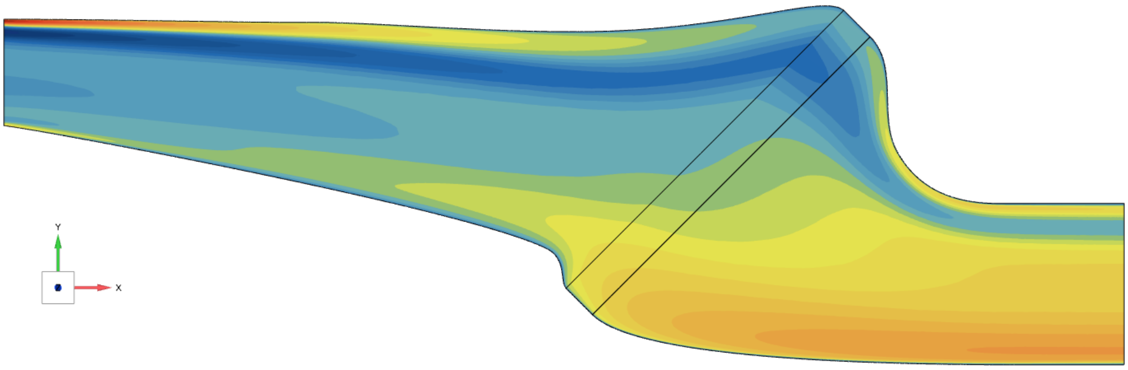

(a) Tangential velocity plot for long ICD using 2D axisymmetric-swirl model.

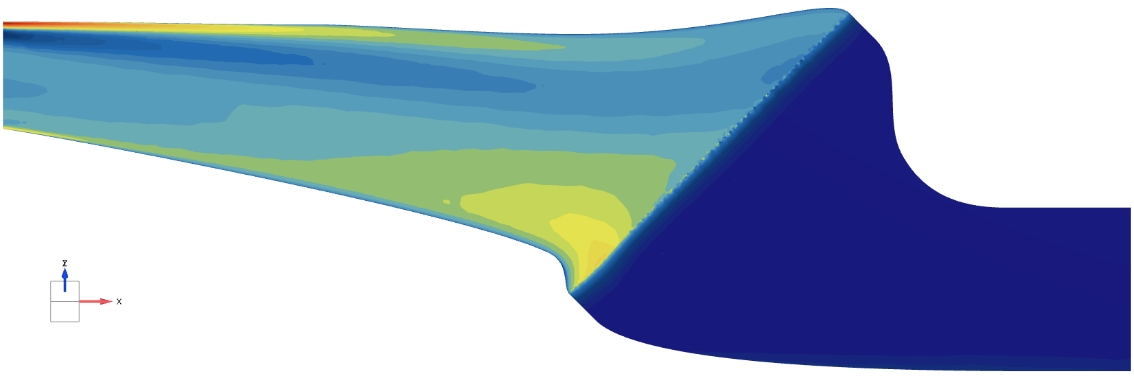

(b) Tangential velocity plot for long ICD using 3D model.

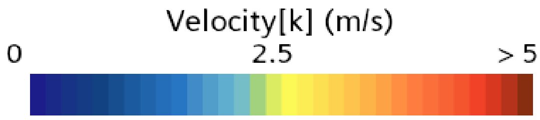

Figure 4.4: Comparison of tangential velocity contours for the long ICD geometry obtained using the 2D axisymmetric-swirl model and the full 3D model. The tangential velocity scale used in both plots is shown below.

4.4 Diffuser performance

The two sections in this chapter covers the results for the pressure recovery coefficient mentioned in chapter 2.2, and the impact of the HEX on the ICD flow.

4.4.1 Pressure recovery

To quantify the performance of the diffuser duct the pressure recovery coefficient C_{pr}, introduced in equation 2.3 is used. The results presented in table 4.4 show a notable difference between the two diffuser geometries, the long geometry appears to benefit significantly more from the inlet swirl than the short geometry does, up to 1% increase in C_{pr}. Despite the short geometry having a slightly higher inlet swirl velocity as showed in table 3.4, the increase in C_{pr} is at most 0.22% while the 2D swirl model actually predicts a decrease in C_{pr}. This indicates that the less aggressive duct design can benefit more from inlet swirl which appears to lead to more efficient diffusion. This observation aligns with previously presented diffuser theory which shows that a diffuser closer to stall is more sensitive to swirl. It is likely that the less aggressive diffuser design is therefore able to benefit more from the inlet swirl since it is not as close to stall as the more aggressive one.

Table 4.3: Pressure recovery coefficient for diffuser duct using each respective CFD setup.

Case	C_{pr}
Long 2D	0.6993
Long 2D swirl	0.7040
Long 3D	0.7095
Short 2D	0.6938
Short 2D swirl	0.6930
Short 3D	0.6960

4.4.2 Heat exchanger stabilization

When observing the differences between the streamline velocity contours for each ICD geometry in figures 4.5 and 4.6, the impact the HEX has on the flow is clearly visible. For both ICD geometries the duct with a HEX present, the flow stays attached to the duct walls and avoids the major separation that is present in the ducts without heat exchangers. This indicates that the HEX has a stabilizing effect and helps suppress flow separation that would otherwise occur due to the strong curvature and high area ratio of the diffuser ducts. This further aligns with observations made in research on HEX integration in airfoils using 2D numerical simulations [8].

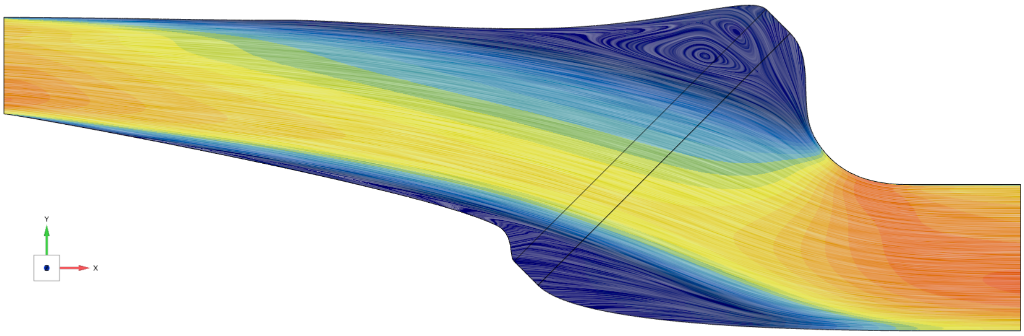

(a) Long ICD geometry without HEX.

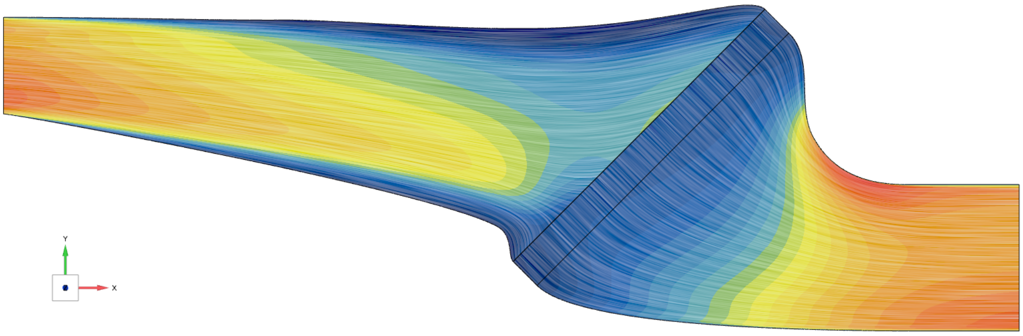

(b) Long ICD geometry with HEX.

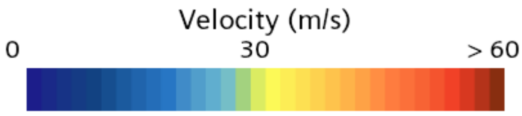

Figure 4.5: Comparison of streamline contour plots for the long ICD geometry with and without HEX.

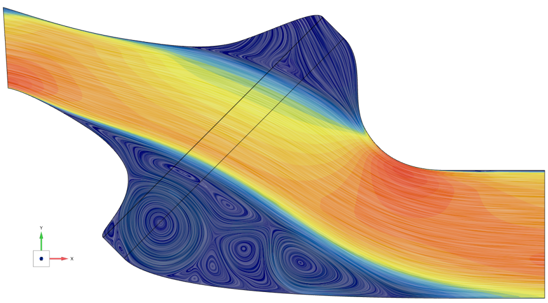

(a) Short ICD geometry without HEX.

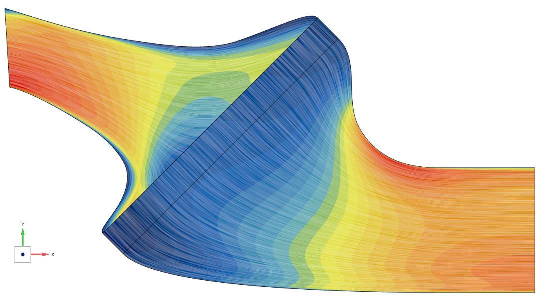

(b) Short ICD geometry with HEX.

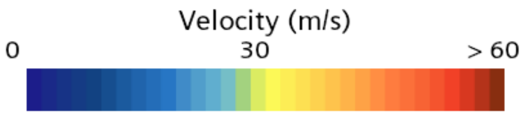

Figure 4.6: Comparison of streamline contour plots for the short ICD geometry with and without HEX.

Further insight into the impact of HEX integration in the ICD can be gained by looking at table 4.4 and comparing the C_{pr} of the ducts with HEXs to the C_{pr} of the clean ducts. For the long ICD geometry the clean duct suffers from a decrease in pressure recovery of approximately 27% compared to the duct with a HEX. For the short ICD the reduction is significantly higher at 54% lower pressure recovery for the clean duct. This significant difference in performance drop when removing the HEX can be attributed to the fundamental design of each diffuser duct. By comparing the geometric parameters for each diffuser duct in table 3.1, it can be concluded that the long diffuser geometry has a L/D_t ratio that is 2.4 times larger compared to the short diffuser, while having a slightly lower AR. This means that the curvature of the long diffuser geometry is significantly weaker compared to the short diffuser which significantly reduces the amount of flow separation that can occur while also allowing the flow more time to develop and thus delaying flow separation. In contrast the flow at the inlet of the short diffuser has very little distance to develop before encountering very strong curvature, especially at the hub wall which causes a jet like flow surrounded by large recirculation zones. Overall the long diffuser geometry is closer to a conventional design which reduces the performance drop that is observed when the HEX is removed. A key observation from this comparison is that the integration of a HEX in an ICD allows for significantly higher area ratios and shorter duct lengths, while maintaining good pressure recovery. It is also interesting that the shorter duct which in a conventional clean configuration would perform significantly worse than the long design, can perform nearly as well with the HEX present.

Table 4.4: Pressure recovery coefficients of ICDs with a HEX present compared to a clean duct for each ICD geometry, using 2D simulation without swirl.

Case	C_{pr}
Long 2D	0.6993
Long 2D no HEX	0.5077
Short 2D	0.6938
Short 2D no HEX	0.3235

5

Conclusion

This study investigated the aerodynamic performance of two intermediate compressor duct (ICD) geometries with integrated heat exchangers using two-dimensional axisymmetric, two-dimensional axisymmetric-swirl, and three-dimensional CFD simulations. The results showed that duct geometry has a significant influence on pressure losses, with the shorter and more aggressive diffuser configuration consistently producing higher losses than the longer geometry. Comparisons between simulation approaches demonstrated that 3D simulations predict higher total pressure losses than both 2D models but also higher pressure recovery coefficients. This highlights the importance of three-dimensional flow effects when analyzing swirling diffuser flows. While inlet swirl was found to slightly improve diffuser pressure recovery, its overall impact on total pressure losses was relatively small. The integrated heat exchanger was shown to have a stabilizing effect on the flow by suppressing separation within the diffuser, which aligns with previous research in the field. This allowed even highly aggressive diffuser geometries to maintain good aerodynamic performance. This indicates that integrated heat exchangers could provide new design opportunities for shorter diffuser ducts with stronger curvature, which could be useful for designing more compact aero engines. One important observation is that the 2D simulations consistently underpredicted the pressure recovery coefficient of the studied diffusers compared to 3D. Another important difference is that the 2D-swirl simulation does not model capture the swirl dissipation over the heat exchanger, which is important for downstream components. Overall, the study indicates that 2D models provide useful preliminary results at a low computational cost, but full 3D simulations can be useful to accurately capture important flow structures and pressure-loss mechanisms in ICDs with integrated heat exchangers.

Bibliography

[1] Anders Lundbladh. Chalmers University of Technology (2025). MMS175 Aerospace Propulsion, guest lecture from GKN Aerospace. “Future aircraft engines & the environment”, Gothenburg, Sweden.

[2] Mital, Subodh K. et al. “Review of Current State of the Art and Key Design Issues With Potential Solutions for Liquid Hydrogen Cryogenic Storage Tank Structures for Aircraft Applications”. NASA technical report (2006). URL: https://ntrs.nasa.gov/citations/20060056194

[3] Alexandre Capitao Patrao, Isak Jonsson, Carlos Xisto, Anders Lundbladh, Tomas Grönstedt. “Compact heat exchangers for hydrogen-fueled aero engine intercooling and recuperation”. In: *Applied Thermal Engineering* 243 (Apr. 2024), p. 122538. ISSN: 1359-4311. DOI: 10.1016/j. URL: https://doi.org/10.1016/j.applthermaleng.2024.122538.

[4] Britchford, KM, Carrotte, JF, Stevens, SJ, & McGuirk, JJ. "The Development of the Mean Flow and Turbulence Structure in an Annular S-Shaped Duct. “Proceedings of the ASME 1994 International Gas Turbine and Aeroengine Congress and Exposition”. Volume 1: Turbomachinery. The Hague, Netherlands. June 13–16, 1994. V001T01A144. ASME. URL: https://doi.org/10.1115/94-GT-457

[5] Reneau, L. R. and Johnston, J. P. and Kline, S. J. “Performance and Design of Straight, Two-Dimensional Diffusers”. In *Journal of Basic Engineering* 89 (Mar. 1967),p. 141. ISSN: 0021-9223. DOI = 10.1115/1.3609544. URL: https://doi.org/10.1115/1.3609544

[6] Jonsson, I., Ranman, R., Capitao Patrao, A. et al (2022). Effect of heat exchanger integration in aerodynamic optimization of an aggressive S-duct. ICAS PROCEEDINGS, 2022

[7] Jonsson, I., Xisto, C., Lejon, M. et al (2021). “Design and pre-test evaluation of a low-pressure compressor test facility for cryogenic hydrogen fuel integration”. Proceedings of the ASME Turbo Expo, 2A-2021. URL: http://dx.doi.org/10.1115/GT2021-58946

[8] Drela, M. “Aerodynamics of Heat Exchangers for High-Altitude Aircraft.” Journal of Aircraft, American Institute of Aeronautics and Astronautics (AIAA), 1996. doi: 10.2514/3.46919.

[9] Elias M. V. Siggeirsson (2020). "Aerodynamics of an Aeroengine Intermediate Compressor Duct: Effects from an Integrated Bleed System”. URL: https://research.chalmers.se/publication/516924

[10] Thomson, G., Pratley, D., and Owen, D.. "Intercooling and Regenerating the Modern Marine Gas Turbine Propulsion System," Marine Rail Propulsion Technology Conference, Washington, District of Columbia, United States, June 8, 1987. URL: https://doi.org/10.4271/871379.

[11] Zhao, X., Tokarev, M., Adi Hartono, E., Chernoray, V., and Grönstedt, T. (November 22, 2016). “Experimental Validation of the Aerodynamic Characteristics of an Aero-engine Intercooler”. ASME. J. Eng. Gas Turbines Power. May 2017; 139(5): 051201. URL: https://doi.org/10.1115/1.4034964

[12] Siemens (Feb 25, 2025). “A new user’s guide to Simcenter STAR-CCM+ simulation (Part 3/5): Meshing”. Siemens Community article. URL: https://community.sw.siemens.com/s/article/A-new-user-s-guide-to-STAR-CCM-simulation-Part-3-5-Meshing

[13] Siemens (Apr 30, 2025). “What is the benefit of a polyhedral mesh?”. Siemens Community article. URL: https://community.sw.siemens.com/s/article/JC-4-332

A

Inlet boundary conditions

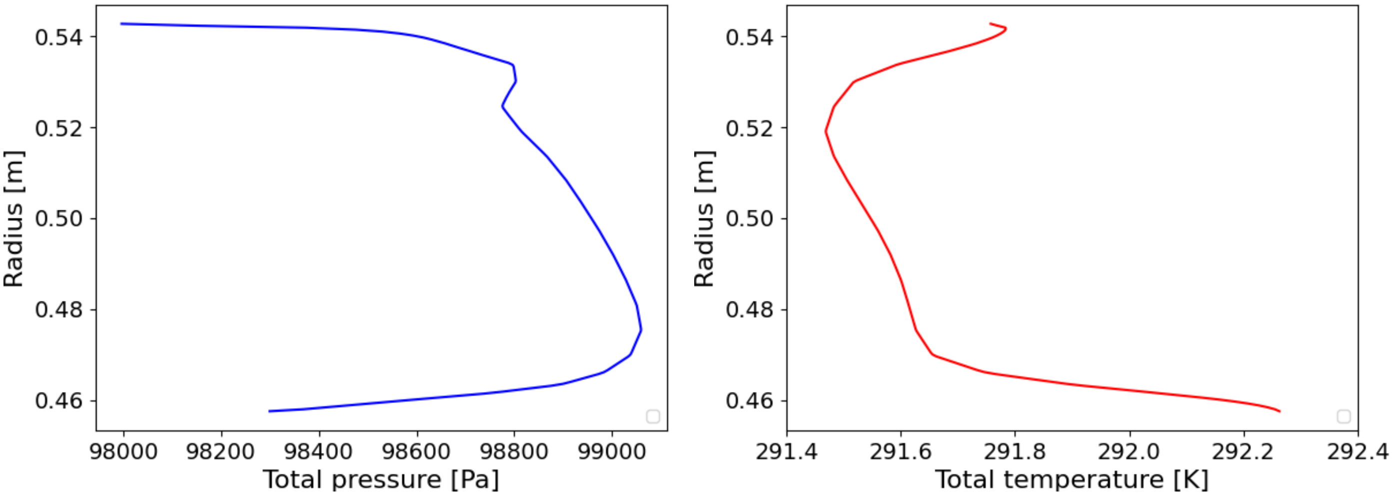

(a) Radial total pressure profile.

(b) Radial total temperature profile.

Figure A.1: Radial inlet profiles for total temperature and pressure, long geometry.

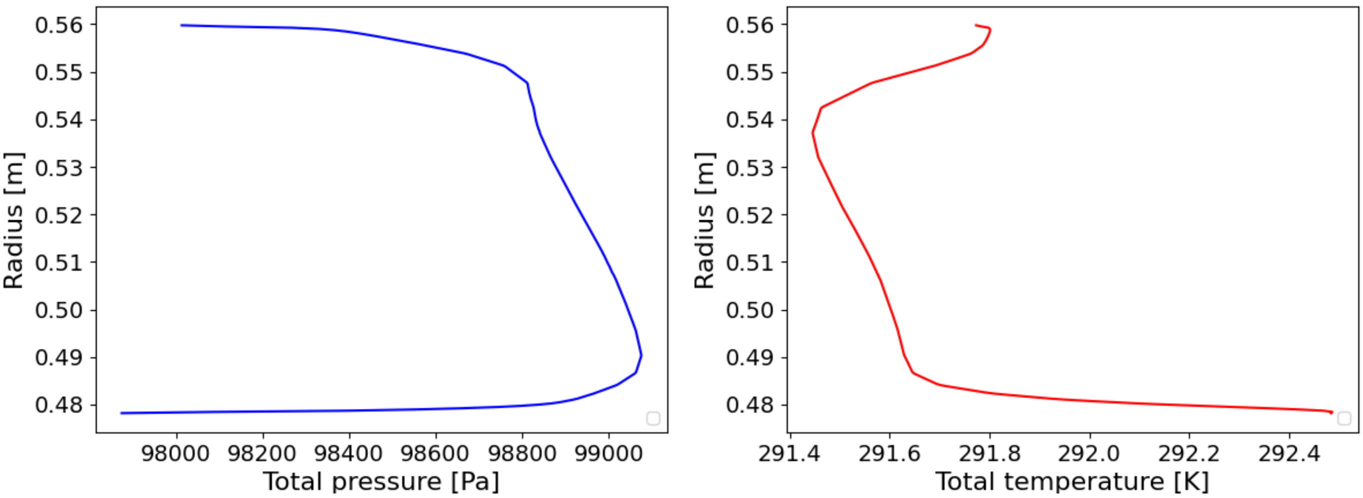

(a) Radial total pressure profile.

(b) Radial total temperature profile.

Figure A.2: Radial inlet profiles for total temperature and pressure, short geometry.

DEPARTMENT OF MECHANICS AND MARITIME SCIENCES
CHALMERS UNIVERSITY OF TECHNOLOGY
Gothenburg, Sweden
www.chalmers.se